The 2009 IEEE/RSJ International Conference on
Intelligent Robots and Systems
October 11-15, 2009 St. Louis, USA

# Experimental Studies of A Teleoperator System with Projection-Based Force Reflection Algorithms

Ilia G. Polushin, Peter X. Liu, and Chung-Horng Lung

*Abstract*— **Results of experimental studies of a teleoperator system with projection-based force reflection algorithms in the presence of communication constraints are presented. It is demonstrated that, using the projection-based force reflection algorithms, the admissible force reflection gain can be substantially increased without loosing the overall stability, which confirms the earlier theoretical results. It is also shown that this improvement is achieved without transparency deterioration.**

## I. Introduction

The trade-off between stability and high force reflection gain is one of the most significant and hard-to-solve problems in bilateral teleoperation with communication delay. Higher force reflection gain provides the human operator with stronger haptic feeling of the interaction with the remote environment; however, it also leads to instability due to increasing the closed-loop gain. In the presence of communication delay, the instability problem becomes more severe, since delays destroy natural passivity of the teleoperator system, which may result for instability for even lower values of the force reflection gain. The approaches proposed in the literature [1]–[3] generally improve stability at the expense of different forms of transparency deterioration. The approach proposed in [4], although does not lead to transparency deterioration, is based on certain assumptions which seem to be hard to justify; for example, it is implicitly assumed that the human operator demonstrates no reaction to the deviation of master's trajectory created by the force reflection term.

The projection-based force reflection algorithms for bilateral teleoperation with communication constraints were introduced in [5] and further developed in [6], [7]. The central idea of these algorithms is to decompose the reflected force into the component compensated by the human hand (and therefore immediately felt by the human operator) and the residual uncompensated component which is solely responsible for creation of the induced master motion and the resulting instability; the latter is subsequently attenuated. Theoretical studies as well as simulations presented in the above references indicate that the projection-based force reflection algorithms may significantly improve admissible force reflection gain without loosing the overall stability in bilateral teleoperation with network-induced communication constraints.

This paper presents, for the first time, results of experimental evaluation of the projection-based force reflection algorithms. The main question addressed in our study is the following: does the use of the projection-based force reflection algorithms lead to improvement in terms of force-reflection gain without loosing stability of the teleoperator system? To answer this question, we performed a set of experiments where the teleoperator system makes a hard contact with the environment, and compared the responses of the system with projection-based force reflection algorithm and the analogous system with direct force reflection, for different values of the force reflection gain as well as different communication delay characteristics. The results of our experiments clearly show that the use of projection-based force reflection algorithms leads to significant improvement in admissible force reflection gain. This improvement is achieved in the case of negligible communication delay as well as in the case of large irregular communication delays; in the latter case, however, the improvement appears to be more dramatic. We also address the transparency issue and show that the mentioned improvement is achieved without paying a price in terms of transparency deterioration; namely, the force response felt by the human operator is virtually indistinguishable from the one generated on the slave side.

The paper is organized as follows. Sections II, III, and IV describe the control algorithms, the force reflection algorithm, and the design of the human force observer, respectively. In section V, description of the experimental setup is presented. Experimental results are discussed in section VI, and concluding remarks are given in section VII.

## II. Teleoperator system

We consider a teleoperator system that consists of a master and a slave manipulators described by the following set of Euler-Lagrange equations

$$H_m\ddot{q}_m + C_m\dot{q}_m + G_m = u_m + f_h - \hat{f}_r, \tag{1}$$

$$H_s\ddot{q}_s + C_s\dot{q}_s + G_s = u_s - f_e. \tag{2}$$

Here, $q_m$, $q_s$ are positions of the master and the slave manipulators, $H_i := H_i(q_i)$ are matrices of inertia, $C_i := C_i(q_i, \dot{q}_i)$ are matrices of Coriolis/centrifugal forces, and $G_i := G_i(q_i)$ are vectors of potential forces of the master ($i = m$) and the slave ($i = s$) manipulators, respectively; here and below, the arguments of $H_i$, $C_i$ and $G_i$ are omitted for brevity. Also, $f_h$ is the force (torque) applied by the

I. G. Polushin is with the Department of Electrical and Computer Engineering, University of Western Ontario, London, ON, N6A 5B9, Canada, E-mail: ipolushin@eng.uwo.ca. P. X. Liu, and C.-H. Lung are with the Department of Systems and Computer Engineering, Carleton University, 1125 Colonel By Drive, Ottawa, ON, K1S 5B6, Canada, E-Mail: {xpliu,chlung}@sce.carleton.ca. This work is partially supported by the Natural Sciences and Engineering Research Council (NSERC) of Canada and the Canada Research Chairs program.

human operator to the master, $f_e$ is the environmental force (torque) applied to the slave, $\hat{f}_r$ is the force reflection term on the master side, and $u_m, u_s$ are the control inputs of the master and the slave respectively. The dynamics of the master (1) and the slave (2) manipulators are assumed to satisfy a set of standard properties described, for example, in [8, Section 2.1]. The master controller implements the following "PD+gravity compensation" algorithm

$$u_m = G_m - K_m \left( \dot{q}_m + \Lambda_m q_m \right), \tag{3}$$

where $K_m, \Lambda_m \in \mathbb{R}^{n \times n}$ are symmetric positive definite matrices. The slave control algorithm has a form

$$\begin{aligned} u_s &= H_s \left( \dot{\xi}_2 + \Lambda_s (\dot{\xi}_1 - \dot{q}_s) \right) + C_s \left( \xi_2 + \Lambda_s \left( \xi_1 - q_s \right) \right) \\ &\quad + G_s - K_s \left( \dot{q}_s - \xi_2 + \Lambda_s \left( q_s - \xi_1 \right) \right), \end{aligned}$$

where $K_s, \Lambda_s \in \mathbb{R}^{n \times n}$ are symmetric positive definite matrices, $\hat{q}_m$ is the master position transmitted to the slave side with communication delay $\tau_f(t)$, *i.e.*,

$$\hat{q}_m(t) := q_m \left( t - \tau_f(t) \right), \tag{4}$$

and $\xi_1, \xi_2 \in \mathbb{R}^n$ are estimates provided by the following "dirty-derivative" filter

$$\begin{aligned} \dot{\xi}_1 &= \xi_2 + g \alpha_1 \left( \hat{q}_m - \xi_1 \right), \\ \dot{\xi}_2 &= g^2 \alpha_0 \left( \hat{q}_m - \xi_1 \right), \end{aligned} \tag{5}$$

where $\alpha_0$, $\alpha_1$ are positive constants such that the roots of $p(s) = s^2 + \alpha_1 s + \alpha_0$ have negative real parts, and $g > 0$. The purpose of filter (5) is to provide a smooth approximation of the (possibly discontinuous due to irregular communication) delayed master position $\hat{q}_m$, as well as estimates for its derivatives, while the slave control law (4) guarantees tracking of the reference trajectory provided by the filter.

## III. Force Reflection Algorithm

In this work, we address a force reflection scheme where the force reflected to the motors of the master $\hat{f}_r$ is described according to the formula

$$\hat{f}_r = \alpha \hat{f}_{env} + (1 - \alpha) \hat{\phi}_{env}. \tag{6}$$

In the above formula, $\hat{f}_{env}$ is the force signal that is arrived directly from the slave subsystem, $\hat{\phi}_{env}$ is the signal generated by the projection-based force reflection algorithm described below, and $\alpha \in [0, 1]$ is a weighting coefficient. The direct force reflecting term $\hat{f}_{env}$ is a delayed version of the force reflection signal $f_{env}$ generated on the slave side, *i.e.*,

$$\hat{f}_{env}(t) = f_{env}(t - \tau_b(t)),$$

where $\tau_b(t)$ is the delay in the backward (from slave to master) communication channel. In our experiments, we address the position-error based scheme, where the force reflecting signal $f_{env}$ is set to be proportional to the position error on the slave side,

$$f_{env} = K_f \left( q_s - \xi_1 \right),$$

where $K_f \geq 0$ is the force reflection gain. On the other hand, the signal $\hat{\phi}_{env}$ is obtained using the projection-based force reflection algorithm, as follows

$$\hat{\phi}_{env} := \operatorname*{Sat}_{[0,1]} \left\{ \frac{\hat{f}_{env}^T \bar{f}_h}{\max \left\{ \left| \bar{f}_h \right|^2, \epsilon_1 \right\}} \right\} \bar{f}_h, \tag{7}$$

where $\bar{f}_h$ is an estimate of the human force applied to the master manipulator, $\epsilon_1 > 0$ is a sufficiently small constant, and $\operatorname*{Sat}_{[a,b]}\{x\} := \max\{a, \min\{x, b\}\}$. Algorithm (7) calculates the component (denoted by $\hat{\phi}_{env}$) of the reflected force that is directly compensated by the human hand force and, therefore, is immediately felt by the human operator. According to (6), $\hat{\phi}_{env}$ is reflected with gain 1; the residual component $\hat{f}_{env} - \hat{\phi}_{env}$ of the reflected force is attenuated with gain $\alpha \in [0, 1]$.

## IV. Force Observer Design

Algorithm (7) utilizes an estimate $\hat{f}_h$ of the force $f_h$ applied by the human operator to the master manipulator. If a direct force measurement on the master side is not available, $\hat{f}_h$ can be obtained using some sort of input estimation technique. In our experiments, we use a high gain input observer designed according to the following method [9]. Suppose we deal with a system of the form $\dot{z} = y + u$, where $z$ and $y$ are known (measured) signals and $u$ is an unknown input to be estimated. Then, the following input observer

$$\begin{aligned} \dot{w} &= -\gamma w + \gamma y + \gamma^2 z, \\ \bar{u} &= \gamma z - w, \end{aligned} \tag{8}$$

provides an estimate $\bar{u}$ of the unknown input $u$, where $w$ is an auxiliary variable, and $\gamma > 0$ is an observer gain which determines the transient response as well the ultimate bound of the estimation error. In the case of the master manipulator described by (1), signals $z$, $y$, and $u$ can be chosen as follows: $z = H_m \dot{q}_m$, $u = f_h$, and $y = \dot{H}_m \dot{q}_m - C_m \dot{q}_m - G_m - \hat{f}_r + u_m$, where $\dot{H}_m \in \mathbb{R}^{n \times n}$, $\dot{H}_m^{\{ij\}} = \left( \partial H_m^{\{ij\}} / \partial q_m \right)^T \dot{q}_m$, $i, j \in \{1, \ldots, n\}$, and $u_m$ is the master control input determined by the control algorithm used (here and below, arguments of $H_m$, $\dot{H}_m$, *etc.*, are omitted for brevity). The above choice of $z$, $y$, $u$ results in the observer of the form

$$\begin{aligned} \dot{w} &= -\gamma w + \gamma^2 H_m \dot{q}_m \\ &\quad + \gamma \left( \dot{H}_m \dot{q}_m - C_m \dot{q}_m - G_m - \hat{f}_r + u_m \right), \\ \bar{f}_h &= \gamma H_m \dot{q}_m - w. \end{aligned}$$

In our experiments, the above observer provides an estimate of the human force applied to the motors of the master device.

## V. Experimental Setup and Modelling

The telerobotic system used in our experiments is shown in Figure 1. It includes two Phantom Premium 1.5A robotic arms with 3 degrees of freedom positional sensing which are provided by SensAble Technologies, Inc.. The master

manipulator is equipped with standard passive stylus and thimble gimbal, while the slave has a marker attached to its last link. As a preliminary step, modelling and parameter identification procedures of the Phantom Premium 1.5A devices were performed. As a result of these procedures, the following model of the Phantom Premium 1.5A is obtained as follows

$$\begin{bmatrix} M_{11} & 0 & 0 \\ 0 & M_{22} & M_{23} \\ 0 & M_{32} & M_{33} \end{bmatrix} \begin{bmatrix} \ddot{q}_1 \\ \ddot{q}_2 \\ \ddot{q}_3 \end{bmatrix} + \begin{bmatrix} C_{11} & C_{12} & C_{13} \\ C_{21} & C_{22} & C_{23} \\ C_{31} & 0 & 0 \end{bmatrix} \begin{bmatrix} \dot{q}_1 \\ \dot{q}_2 \\ \dot{q}_3 \end{bmatrix}$$
$$+ \begin{bmatrix} K_{fv1}\dot{q}_1 + K_{fc1}\,\mathrm{sign}\,\dot{q}_1 \\ G_2 + K_{fv2}\dot{q}_2 + K_{fc2}\,\mathrm{sign}\,\dot{q}_2 \\ G_3 + K_{fv3}\dot{q}_3 + K_{fc3}\,\mathrm{sign}\,\dot{q}_3 \end{bmatrix} = \begin{bmatrix} \tau_1 \\ \tau_2 \\ \tau_3 \end{bmatrix},$$

where $\tau_i$ are joint torques, $M_{ij}$ are the elements of inertia matrix, $C_{ij}$ are elements of the matrix of Coriolis and centrifugal forces (torques), $G_i$ are elements of the gravity vector, and $K_{fv}$, $K_{fc}$ are viscous and Coulomb friction coefficients, respectively. In the above equations,

$$\begin{aligned}
M_{11} &= \pi_1 + \pi_2 \cos^2 q_2 + (\pi_3 + \pi_5)\sin^2 q_3 \\
&\quad +2\pi_6 \cos q_2 \sin q_3, \\
M_{22} &= \pi_4 + \pi_5 - 2\pi_6 \sin(q_2 - q_3), \\
M_{23} &= M_{32} = \pi_5 - \pi_6 \sin(q_2 - q_3), \\
M_{33} &= \pi_5, \\
C_{11} &= -(\pi_2 \sin q_2 \cos q_2 + \pi_6 \sin q_2 \sin q_3)\dot{q}_2 \\
&\quad +((\pi_3 + \pi_5)\sin q_3 \cos q_3 + \pi_6 \cos q_2 \cos q_3)\dot{q}_3, \\
C_{12} &= -(\pi_2 \sin q_2 \cos q_2 + \pi_6 \sin q_2 \sin q_3)\dot{q}_1, \\
C_{13} &= ((\pi_3 + \pi_5)\sin q_3 \cos q_3 + \pi_6 \cos q_2 \cos q_3)\dot{q}_1, \\
C_{21} &= (\pi_2 \sin q_2 \cos q_2 + \pi_6 \sin q_2 \sin q_3)\dot{q}_1, \\
C_{22} &= \pi_6 \cos(q_2 - q_3)\,(\dot{q}_3 - \dot{q}_2) \\
C_{23} &= \pi_6 \cos(q_2 - q_3)\,(\dot{q}_2 - \dot{q}_3) \\
C_{31} &= -(\pi_3 + \pi_5)\sin q_3 \cos q_3 \dot{q}_1 - \pi_6 \cos q_2 \cos q_3 \dot{q}_1,
\end{aligned}$$

$$G_2 = \pi_7 \cos q_2,\ G_3 = \pi_8 \sin q_3,\ K_{fv1} = \pi_9,\ K_{fv2} = \pi_{10},$$

$$K_{fv3} = \pi_{11},\ K_{fc1} = \pi_{12},\ K_{fc2} = \pi_{13},\ K_{fc3} = \pi_{14}.$$

It is worth noting that in the software implementation used in our experiments, the position in joint space is measured in units of radians, while the joint space input (torque) is a numerical value between -32768 to 32767. The parameter identification procedure gives the following values of the parameters $\pi_1, \ldots, \pi_{14}$ of the master manipulator: $\pi_1 = 50$, $\pi_2 = 60$, $\pi_3 = 48$, $\pi_4 = 80$, $\pi_5 = 9$, $\pi_6 = 8$, $\pi_7 = 235$, $\pi_8 = 270$, $\pi_9 = 25$, $\pi_{10} = 22$, $\pi_{11} = 110$, $\pi_{12} = 82$, $\pi_{13} = 160$, $\pi_{14} = 90$. For the slave manipulator, the parameters are identified as follows: $\pi_1 = 32$, $\pi_2 = 34$, $\pi_3 = 20$, $\pi_4 = 74$, $\pi_5 = 1$, $\pi_6 = 2$, $\pi_7 = -926$, $\pi_8 = -685$, $\pi_9 = 15$, $\pi_{10} = 15$, $\pi_{11} = 90$, $\pi_{12} = 80$, $\pi_{13} = 112$, $\pi_{14} = 55$. In all the experiments discussed below, the parameters of control law (3), (4), (5) are chosen as follows: $\Lambda_m = \mathrm{diag}\,\{2, 2, 2\}$, $\Lambda_s = \mathrm{diag}\,\{5, 5, 5\}$, $K_m = \mathrm{diag}\,\{10, 10, 10\}$, $K_s = \mathrm{diag}\,\{300, 300, 300\}$, $g = 10$, $\alpha_1 = 4$, $\alpha_0 = 4$.

## VI. Experimental Results

In the experiments described in this section, the end-effector of the master manipulator is initially located approximately at the origin of the task space coordinate frame; in particular, $x(0) \approx 0\ m$. Starting from approximately $t = 10$ seconds, the human operator quickly moves the end-effector of the master along the negative direction of the X-axis, then returns it back to the origin and immediately releases. Figure 2 shows an example of the movement of the master manipulator which is intended by the human operator. When slave follows the master's trajectory, it hits an obstacle which is located approximately at $x = -0.25\ m$. The obstacle is a rigid wall with very high stiffness. The quick movement together with a contact with a rigid environment create a strong destabilizing effect; the goal of the experiments presented is to evaluate the resulting response of the master-slave teleoperator system, in particular in the presence of communication delay and jitter. More precisely, we compare the responses of the teleoperator system with direct force reflection (which corresponds to $\alpha = 1$ in (7)) with the analogous responses of the system with nonzero weight of the projection-based component in the force reflection term (*i.e.*, $\alpha \in [0, 1)$ in (7)), for different values of force reflection gain as well as different communication delay characteristics.


Fig. 1. Experimental setup

In general, the experimental results clearly indicate that the use of the projection-based component in the force reflection algorithms substantially improve the admissible force-reflecting gain without loosing the overall stability of the teleoperator system. This improvement is achieved in the case of small (negligible) communication delays as well as in the case of significantly large irregular communication delays; however, in the latter case the improvement is somewhat more dramatic. In particular, examples of the teleoperator system's responses in the case of direct force reflection ($\alpha = 1$) and negligible communication delays are presented in Figures 3, 4. As expected, the system is stable for low values of the force reflection gain and unstable for high ones; the border of stability in terms of admissible FR gain in this case lies somewhere between 3000 (still stable, Figure 3) and 4000 (unstable, Figure 4). On the other hand, figure 5 shows the analogous response for $\alpha = 0.5$. (*i.e.*, the weights of the direct component and the projection-based component are equal in the force reflection term) and FR gain$= 4000$. One can see that the response is perfectly stable. An explanation is that, since the operator releases the master

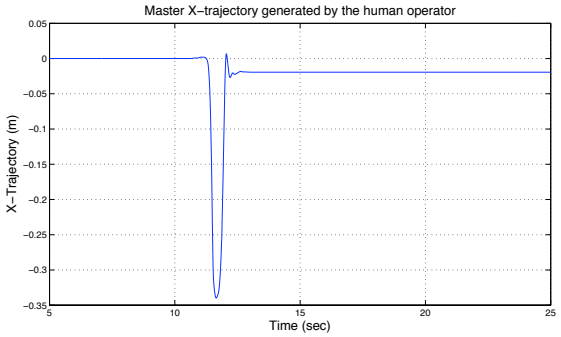


Fig. 2. Example of the master trajectory generated by the human operator

immediately after returning back to origin, the corresponding projection of the reflected force onto the estimated vector of the human force becomes (approximately) zero, and so does the projection based force reflection term, which results in improved stability. The natural question, of course, is how does this type of force reflection affect the transparency of the system; in other words, what would the human operator feel if she/he does not release the master. The answer to this question can be illustrated by figure 6, where, instead of releasing the master, the human operator tries to hold it firmly after returning to the origin. One can see that, in this case, the force reflected to the motors of the master actually follows quite closely the contact force generated on the slave side. The small difference between these force responses can be attributed to the fact that the estimate of the human force is obtained using a high-gain observer that, besides having its own dynamics, is built based on the model which probably has some discrepancy with the actual dynamics of the robot.

In the next set of the experiments, the communication delays in both directions are set to be normally distributed random variables ( $\tau(\cdot) \sim \mathbb{N}\left(T_{av}, \sigma^2\right)$) with mean $T_{av} = 1$ sec, and standard deviation $\sigma = 0.02$ sec. Examples of experimental results for system with direct force reflection ($\alpha = 1$) are shown in Figures 7, 8; these figures correspond to FR gains equal to 1000 and 1500, respectively. Although the qualitative picture remains the same (*i.e.*, the system is stable for low FR gains, and unstable for high ones), the border of stability in this case lies somewhere between 1000 (stable, Figure 7) and 1500 (unstable, Figure 8), which is significantly lower comparing to the case of negligible communication delays. On the other hand, examples of the experimental results for the system with projection-based force reflection algorithm with FR Gain=4000 and $\alpha = 0.3$ are shown in figures 9, 10. In particular, figure 9 represents the experiments where the human operator releases the master immediately after returning back to origin. One can see that the system quickly stabilizes. On the other hand, the transparency properties of the system is illustrated by figure 10, where the human operator holds firmly the master after returning to the origin. Again, one can see that in this case, the force reflected to the hand of the human operator follows closely the actual contact force generated on the slave side, thus confirming that there is virtually no transparency loss. Overall, the experimental data indicate that the use of projection-based force reflection algorithms in bilateral teleoperation, particularly in the presence of communication delays, leads to drastic improvement in admissible force reflection gain without loosing the stability of the overall system.

## VII. Conclusion

In this work, results of experimental investigation of a teleoperator system with projection-based force reflection algorithms are presented. In the experiments performed, we compare responses of a teleoperator system with projection-based force reflection algorithm and a similar system with direct force reflection, for different values of the force reflection gain as well as different communication delay characteristics. The experimental results achieved clearly indicate that the use of projection-based force reflection algorithms, particularly in the presence of significant communication delays, leads to drastic improvement in terms of admissible force reflection gain without loosing the stability of the teleoperator system. Moreover, it is demonstrated that, if the human operator holds the master device firmly, the discrepancy between the contact forces and the reflected forces is negligible, which implies that the above mentioned improvement is achieved without paying the price in terms of transparency deterioration. In the future, it would be promising to study in more details the properties of these algorithms, as well as their applicability to a variety of teleoperation and haptics tasks. In particular, application to three- and four-channels teleoperation architectures may also lead to significant improvements and, therefore, would be of great interest.

## References

[1] B. Hannaford, "A design framework for teleoperators with kinesthetic feedback," *IEEE Transactions on Robotics and Automation*, vol. 5, pp. 426–434, Aug. 1989.

[2] R. W. Daniel and P. R. McAree, "Fundamental limits of performance for force reflecting teleoperation," *International Journal of Robotics Research*, vol. 8, pp. 811–830, 1998.

[3] J. E. Speich, K. Fite, and M. Goldfarb, "A method for simultaneously increasing transparency and stability robustness in bilateral telemanipulation," in *Proceedings of the IEEE International Conference on Robotics and Automation ICRA 2000*, (San Francisco, CA), pp. 2671–2676, Apr. 2000.

[4] K. J. Kuchenbecker and G. Niemeyer, "Induced master motion in force-reflecting teleoperation," *ASME Journal of Dynamic Systems, Measurement, and Control*, vol. 128, no. 4, pp. 800–810, 2006.

[5] I. G. Polushin, P. X. Liu, and C.-H. Lung, "A force-reflection algorithm for improved transparency in bilateral teleoperation with communication delay," *IEEE/ASME Transactions on Mechatronics*, vol. 12, no. 3, pp. 361–374, 2007.

[6] I. G. Polushin, P. X. Liu, and C.-H. Lung, "Projection-based force reflection algorithm for stable bilateral teleoperation over networks," *IEEE Transactions on Instrumentation and Measurement*, vol. 57, no. 9, pp. 1854–1865, 2008.

[7] I. G. Polushin, P. X. Liu, and C.-H. Lung, "Stability of bilateral teleoperators with projection-based force reflection algorithms," in *2008 IEEE International Conference on Robotics and Automation*, (Pasadena, CA), pp. 677–682, May 2008.

[8] M. W. Spong, "Motion control of robot manipulators," in *Handbook of Control* (W. Levine, ed.), pp. 1339–1350, CRC Press, 1996.

[9] A. Stotsky and I. Kolmanovsky, "Application of input estimation techniques to charge estimation and control in automotive engines," *Control Engineering Practice*, vol. 10, pp. 1371–1383, 2002.

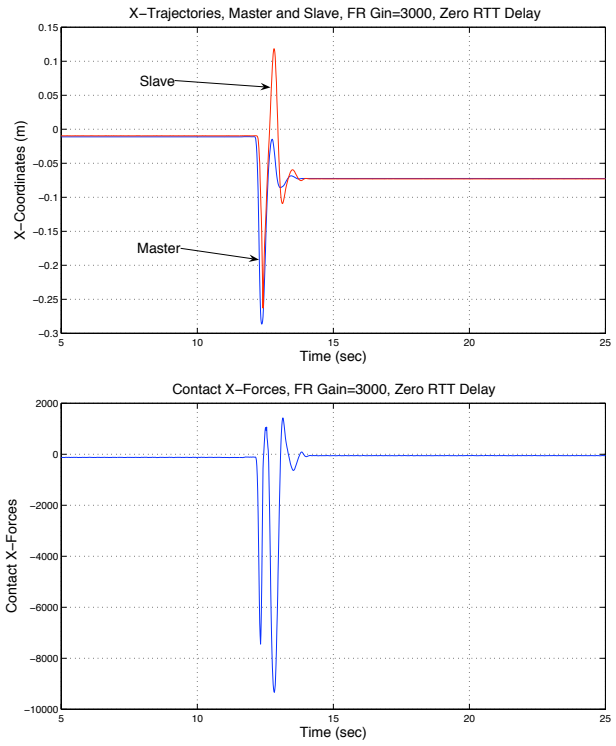


Fig. 3. Direct force reflection ($\alpha = 1$), Delay$\approx$ 0, FR gain=3000: X-trajectories, master and slave (top); Contact X-Forces (bottom)

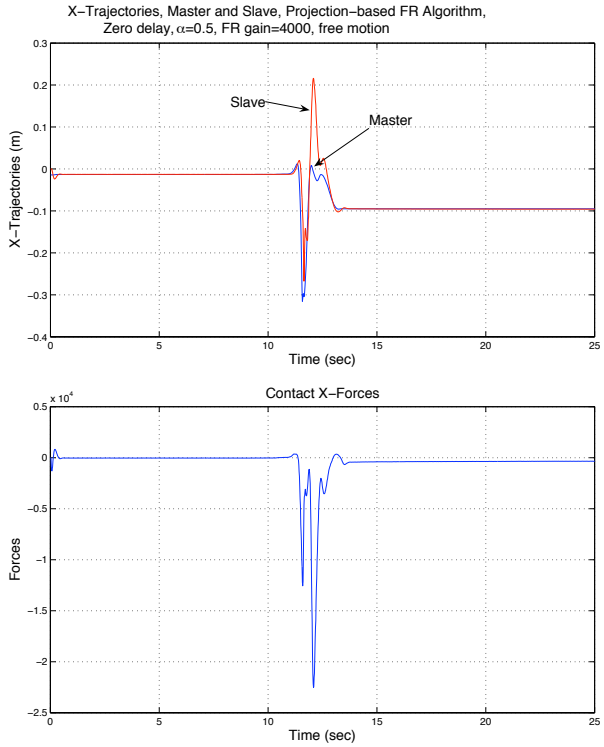


Fig. 5. Projection-based force reflection ($\alpha = 0.5$), Delay$\approx$ 0, FR gain=4000, free motion: X-trajectories, master and slave (top); Contact X-Forces (bottom)

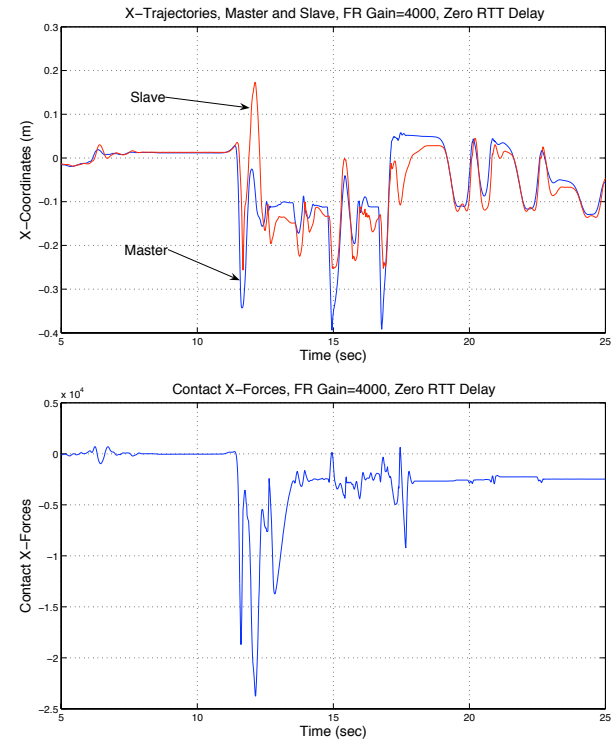


Fig. 4. Direct force reflection ($\alpha = 1$), Delay$\approx$ 0, FR gain=4000: X-trajectories, master and slave (top); Contact X-Forces (bottom)

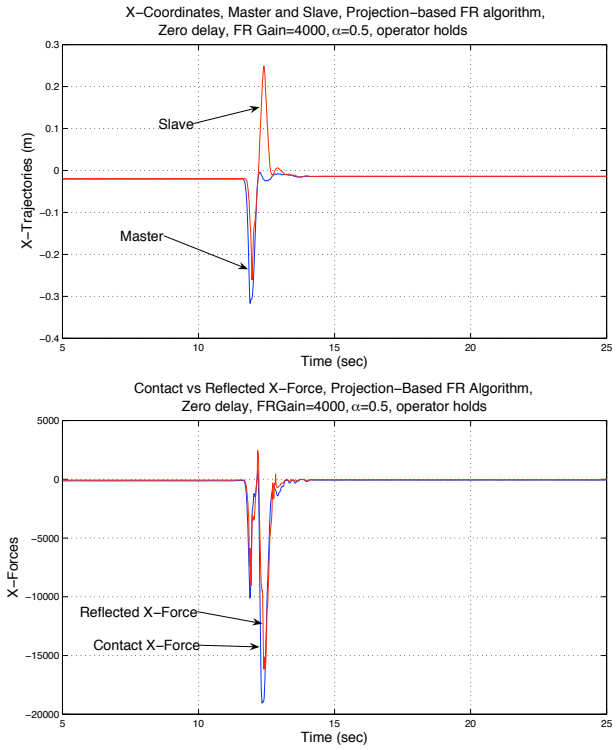


Fig. 6. Projection-based force reflection ($\alpha = 0.5$), Delay$\approx$ 0, FR gain=4000, operator holds: X-trajectories, master and slave (top); Contact X-Forces vs. Reflected X-Forces(bottom)

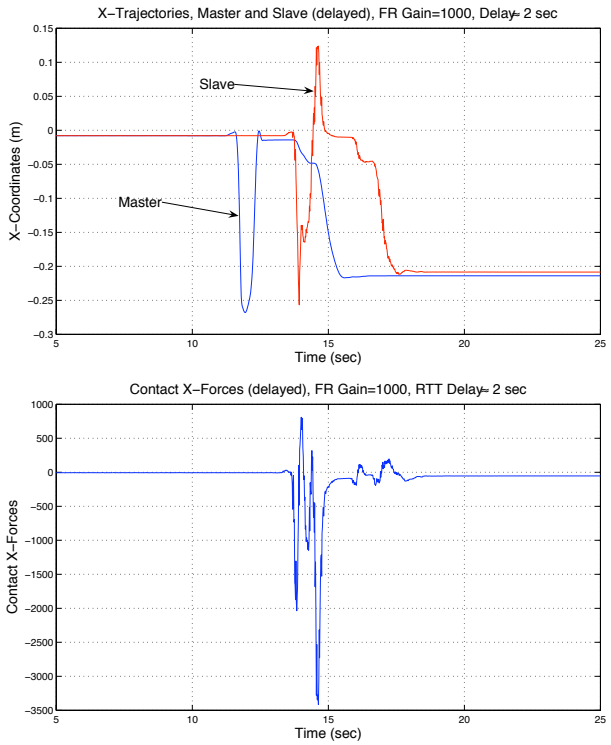


Fig. 7. Direct force reflection ($\alpha = 1$), Delays $\tau_f(\cdot), \tau_b(\cdot) \sim \mathbb{N}\left(T_{av}, \sigma^2\right)$, $T_{av} = 1$ s, $\sigma = 0.02$ s, FR gain=1000: X-trajectories, master and slave (top); Contact X-Forces (bottom)

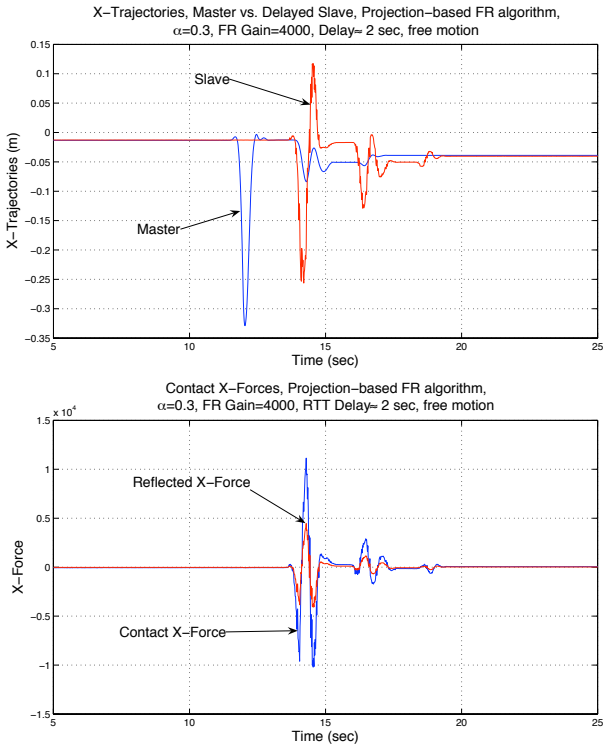


Fig. 9. Projection-based force reflection ($\alpha = 0.3$), Delays $\tau_f(\cdot), \tau_b(\cdot) \sim \mathbb{N}\left(T_{av}, \sigma^2\right)$, $T_{av} = 1$ s, $\sigma = 0.02$ s, FR gain=4000, free motion: X-trajectories, master and slave (top); Contact X-Forces (bottom)

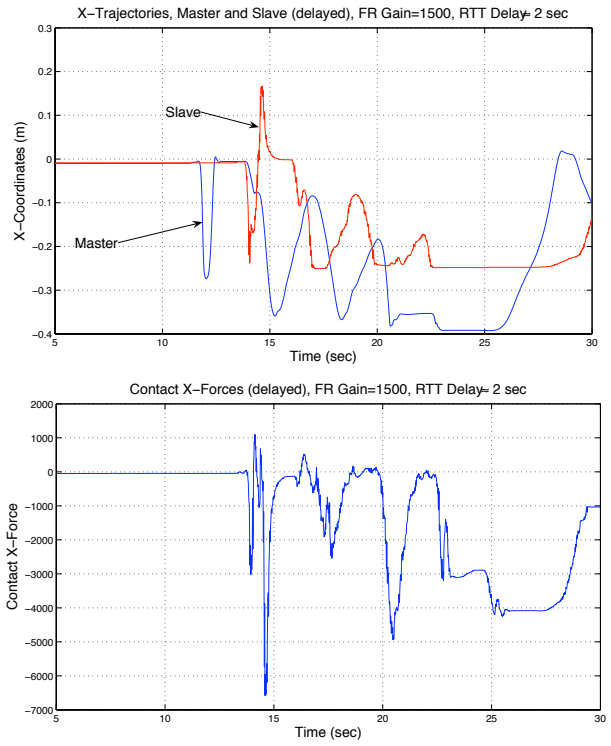


Fig. 8. Direct force reflection ($\alpha = 1$), Delays $\tau_f(\cdot), \tau_b(\cdot) \sim \mathbb{N}\left(T_{av}, \sigma^2\right)$, $T_{av} = 1$ s, $\sigma = 0.02$ s, FR gain=1500: X-trajectories, master and slave (top); Contact X-Forces (bottom)

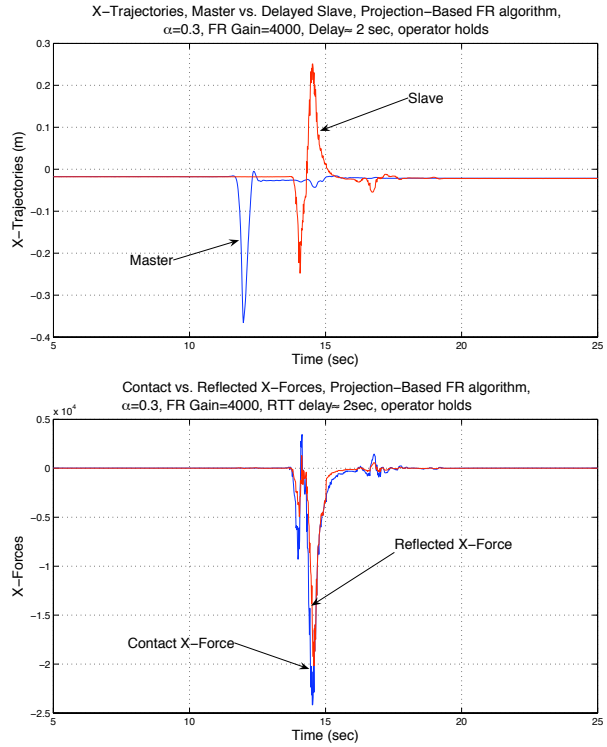


Fig. 10. Projection-based force reflection ($\alpha = 0.3$), Delays $\tau_f(\cdot), \tau_b(\cdot) \sim \mathbb{N}\left(T_{av}, \sigma^2\right)$, $T_{av} = 1$ s, $\sigma = 0.02$ s, FR gain=4000, operator holds: X-trajectories, master and slave (top); Contact X-Forces vs. Reflected X-Forces(bottom)